

Coherent Change Detection with Complex Logarithm Transformation on SAR Imagery

Takehiro HOSHINO

Graduate School of Electro-Communications,

University of Electro-Communications

1-5-1 Chofugaoka Chofu-shi 182-8585 Tokyo, Japan

Email: hoshino@secure.ee.uec.ac.jp

Shouhei KIDERA and Tetsuo KIRIMOTO

Graduate School of Informatics and Engineering,

University of Electro-Communications

1-5-1 Chofugaoka Chofu-shi 182-8585 Tokyo, Japan

Email: kirimoto@ee.uec.ac.jp

Abstract—A satellite-borne SAR (synthetic aperture radar) is quite promising technique for high-resolution geosurface measurement. Recently, the feature extraction method based on the CCD (coherent change detection) has been developed, which detects a small surface change on the geosurface by using the phase relationship between the plural complex SAR images of the same region in different observations. Aiming at fast and accurate detection of the surface change, the logarithm transformation method, has been proposed. This method can determine the appropriate threshold for the change detection, while enhancing the detection probability and suppressing the false alarm rate. However, it does not employ phase information of the estimated coherence function, and its detection probability deteriorates, especially in the case when target has small surface changes. To overcome this problem, a novel transformation index is proposed considering the phase difference of the coherence function. The results from the experiment modeling of geosurface measurement verify the effectiveness of the proposed method, even in the lower SNR (signal to noise ratio) situations.

Keywords; Geosurface measurement, Satelite-borne SAR, CCD.

I. INTRODUCTION

The high-resolution microwave imaging technique known as SAR is very useful in the geosurface measurement, even in cloudy weather or darkness [1]-[3]. The ability to detect a change in targets using remote surveillance is important for the assessment of damage caused by natural disaster. Recently, the CCD method has been developed for the surface change detection, [4], [5], such as in fault or upthrow, which is simply based on the correlation between the plural complex SAR images obtained by temporally different observations for the same region. This technique makes it possible to detect a slight change of geosurface occurred in the interval between plural complex SAR image collections. The coherence function corresponds to a correlation coefficient between the local SAR images, and its value decreases when the target surface is changed. However, this technique requires a considerably high SNR to obtain the accurate coherence [6], [7]. Recently, fast and accurate detection of the surface change, Fisher logarithm transformation method has been proposed [8]. This method determines the appropriate threshold for the change detection

easily. However, it does not employ phase information of the estimated coherence function, and the detection probability deteriorates, especially in the case that the target has small surface changes. To overcome this problem, this paper proposes a novel transformation index by considering the phase difference of the coherence function.

In this paper, the observation model is introduced in Section II, where the coherence function and the system model is defined. Section III shows the conventional and proposed detection indices. Section IV presents the numerical simulation model to evaluate the performance of each index including noisy situations, where white Gaussian noises are numerically added. Finally, the experimental results described in Section V prove that the proposed method attains a high detection performance compared with the conventional method, even in noisy situations.

II. OBSERVATION MODEL AND COHERENCE ESTIMATION OF THE COMPLEX SAR IMAGES

Fig. 1 shows the observation geometry in the experiment. The target is made of clay with 4.8 relative permittivity approximately. The width, depth and thickness of the target are 80 cm, 80 cm and 3 cm, respectively. The incident (offnadir) angle is 50° and the surface roughness is around 5 mm in height. The half of the target surface is changed by small tire trace. The transmission frequency is from 26 GHz to 40 GHz, which is measured by the vector network analyzer. The transmitting and receiving horn antennas are scanned at the height of 1.48 m, where the synthetic aperture length is 1.6 m. The complex SAR image is produced by the back projection method [2], [3]. Table 1 shows the experimental parameters. s_1 and s_2 are defined as the complex SAR images of the target before and after the surface changes are added to the target. The coherence function γ between two SAR images is defined as [4]-[7]

$$\gamma(m, n) = \frac{\sum_{i=0}^{L-1} \sum_{j=0}^{L-1} s_1(m+i, n+j) \cdot s_2^*(m+i, n+j)}{\sqrt{\sum_{i=0}^{L-1} \sum_{j=0}^{L-1} |s_1(m+i, n+j)|^2} \sqrt{\sum_{i=0}^{L-1} \sum_{j=0}^{L-1} |s_2(m+i, n+j)|^2}}, \quad (1)$$

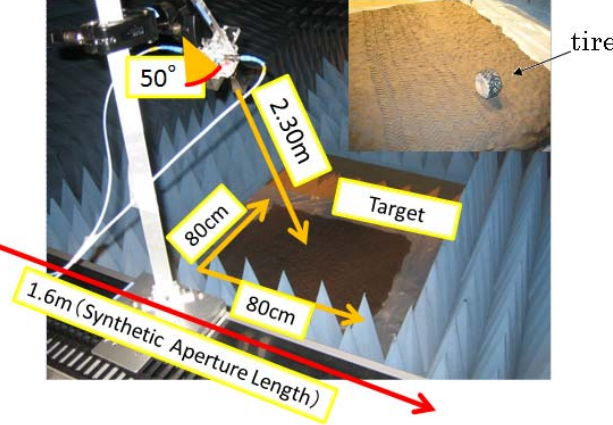


Figure 1. Observation geometry.

TABLE I. EXPERIMENTAL PARAMETERS

Center frequency	33 GHz
Frequency bandwidth	14 GHz
Synthetic aperture length	1.6 m
Target size (length, depth and thickness)	80 x 80 x 3 cm

where (m, n) denotes the x and y coordinates of the SAR image, $*$ is a complex conjugate and L denotes the window size in the correlation. $0 \leq |\gamma| \leq 1$ holds. This function offers surface change detection by evaluating the discrepancy of the amplitude and phase of γ .

III. DETECTION INDEX

A. Conventional Method

As a high-speed detection index, the Fisher logarithm detection index has been proposed, which approximates the probability density function of γ to the Gaussian distribution [8]. This transformation is defined as,

$$\alpha(m, n) = \frac{1}{2} \ln \frac{1 + |\gamma(m, n)|}{1 - |\gamma(m, n)|} \quad (2)$$

However, since this index uses only the absolute value of γ , it distorts the detection probability in the case when the phase of rotates despite the absolute value of γ remained high.

B. Proposed Method

To solve the problem described above, we propose a novel detection index β as

$$\beta(m, n) = \frac{1}{2} \ln \frac{|1 + \gamma(m, n)|}{|1 - \gamma(m, n)|} \quad (3)$$

Substituting $\gamma = A \exp(j\theta)$, Eq. (3) is reformed as

$$\beta(m, n) = \frac{1}{2} \ln \frac{\sqrt{1 - 2A^2 \cos 2\theta + A^4}}{1 - 2A \cos \theta + A^2}, \quad (4)$$

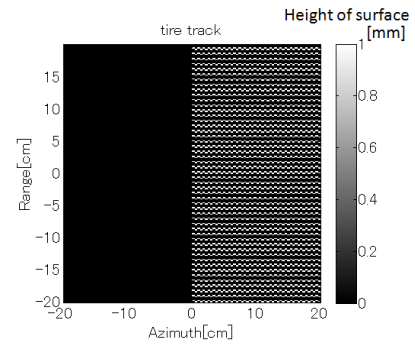


Figure 2. Height distribution of target surface tire model.

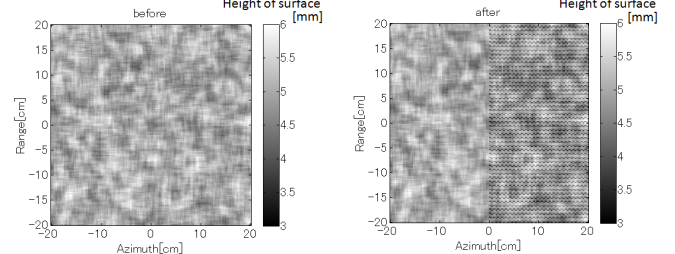


Figure 3. Height distribution of target surface, before (left) and after (right) the tire track was added.

where $A \leq 1$ holds. Eq. (4) indicates that this index calculates the change detection by considering the amplitude and phase difference between the complex SAR images.

IV. PERFORMANCE EVALUATION IN NUMERICAL SIMULATIONS

In numerical simulation, we assume that the rough surface target is composed of multiple scattering points with random amplitudes for simplicity. The received signal from these scattering points is defined as S_k

$$S_k = A_k \exp\left(-j4\pi \frac{f}{c} R_k\right), \quad (5)$$

where k is the number of the scattering points, A_k denotes reflection coefficient, and f is transmitting frequency. c is the speed of radio wave in air and R_k denotes a distance from an antenna to a scattered point for number k . f is swept from 26 GHz to 40 GHz. $A_k = 1$ is assumed in this case. Then, the received signal from the rough surface target S is simply calculated as [9]

$$S = \sum_{k=0}^{N-1} A_k \exp\left(-j4\pi \frac{f}{c} R_k\right), \quad (6)$$

where $N = 40000$ and denotes the total number of scattered points. We obtain a received signal in the time domain by using inverse Fourier transform for S in each antenna location. The target surface is modified by adding the height change using the uniform distribution from 0 cm to 1 cm, and then, it is smoothed by the spatial averaging filter of 2 cm \times 2 cm region.

Fig. 2 shows the target surface with the periodical height

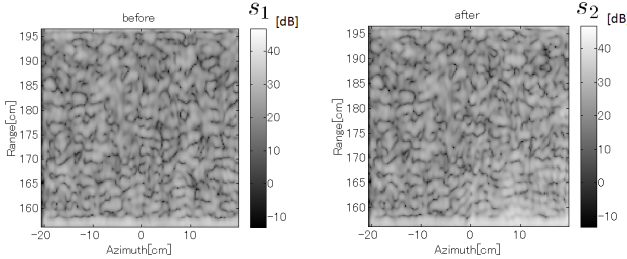


Figure 4. Intensity of the complex SAR images obtained by simulation before (left) and after (right) the tire track was added.

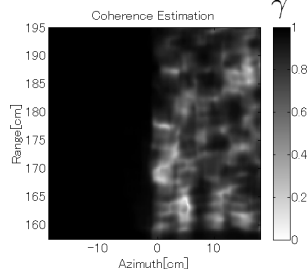


Figure 5. Coherence intensity map of the complex SAR images obtained by noiseless simulation.

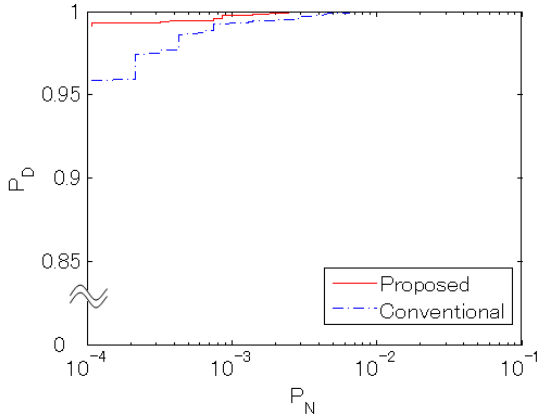


Figure 6. Pn-Pd characteristic with the simulation data in noiseless situation.

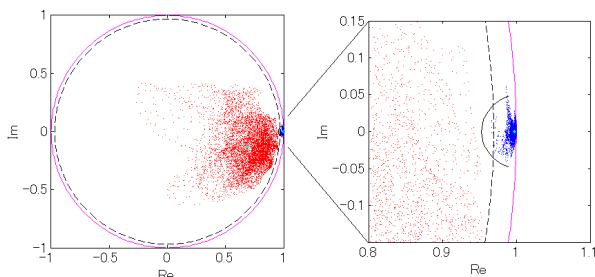


Figure 7. Distribution of γ obtained by numerical simulation in noiseless situation. (The red and blue points show the changed and unchanged target points. The broken and solid boundaries correspond to the conventional and proposed indices, where $P_N = 10^{-3}$ is required).

changes in imitated tire track. The ditch of this track is 1 mm in depth and 8 mm in width. The left and right hand sides of Fig. 3 show the height distribution of the target surfaces, before and after the target surface was changed, respectively.

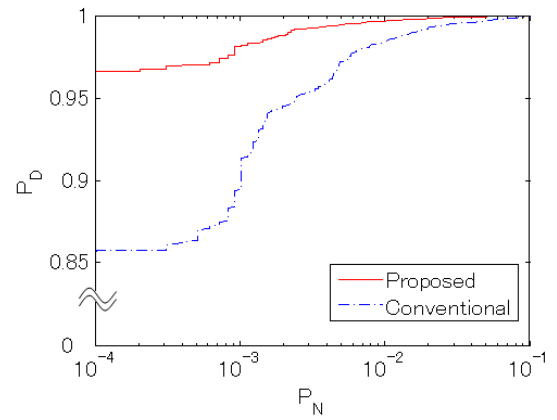


Figure 8. Pn-Pd characteristic with the simulation in noisy situation when SNR=20dB.

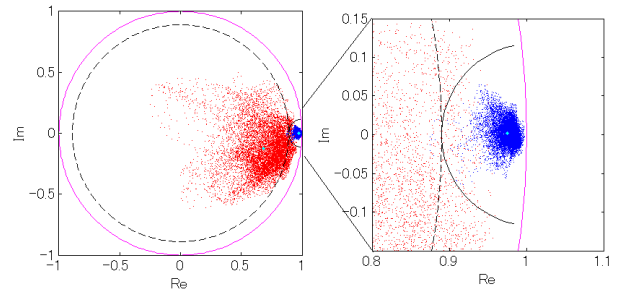


Figure 9. Distribution of γ obtained by numerical simulation in noisy situation when SNR=20dB, and each definition is same as in Fig. 7.

The left and right hand sides of Fig. 4 show the intensities of the complex SAR images before and after the periodical track was added to the surface, respectively. As shown in Fig. 4, it is confirmed that there is not a significant difference between two SAR images. This is because the image intensity has little variation in RCS (radar cross section) by this surface change. On the contrary, Fig. 5 shows the intensity of coherence γ calculated in Eq. (1) between two SAR images shown in Fig. 4, where $L = 3$ cm. The right hand side of this figure successfully illustrates the target region with height changes by calculating the coherence correlation index.

Next, the performance of each method is investigated. Fig. 6 shows the relationship between the false-alarm probability named as P_N and detection probability as P_d in the numerical simulation for each method in noiseless situation. As a result, a significant difference is not examined in Fig. 6. Furthermore, Fig. 7 shows the coherence on the Gaussian plane, where the unchanged area is shown as blue points and the changed area is shown as red points, respectively. Here, the blue points retain higher values and focus around the region of $\gamma = 1$.

Next, we assess the proposed method in noisy situation. The signal powers are calculated with the SAR complex images included in P_s target region as

$$P_s = \frac{1}{MN} \sum_{m=0}^{M-1} \sum_{n=0}^{N-1} s(m, n) \cdot s^*(m, n). \quad (7)$$

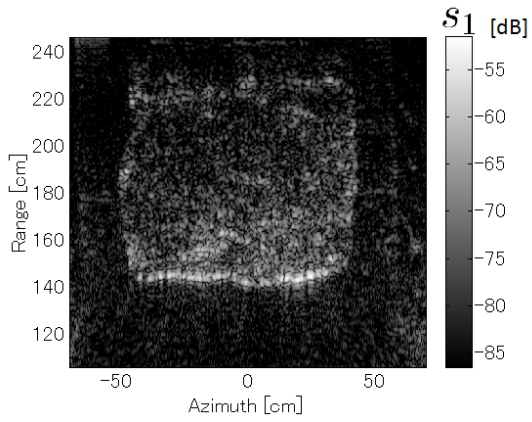


Figure 10. Intensity of the complex SAR images using HH polarized signals before the target surface was changed.

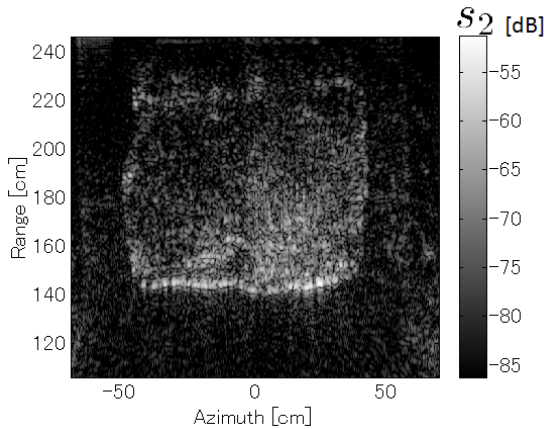


Figure 11. Intensity of the complex SAR images using HH polarized signals after the target surface was changed.

M and N correspond to the target size of SAR image. Then, we obtain a complex SAR image by adding white Gaussian noise. The numerical simulation for each method at SNR=20dB was performed and the characteristic of $P_N - P_D$ in this case is shown in Fig. 8. These results verify that the proposed method improves the detection probability as 8 % at $P_N=10^{-3}$. Fig. 9 shows distribution of γ obtained by numerical simulation in noiseless situation. These red points show the coherence in the target changed region, whereas blue points show the coherence in unchanged target region. This figure shows that the threshold boundary of the proposed method accurately detects the target points with surface changes.

V. PERFORMANCE EVALUATION IN AN EXPERIMENT

This section presents the performance example in the experiment. Figs. 10 and 11 show the SAR images using the HH polarized radiation before and after the target surface was changed, respectively. From these figures, the significant discrepancy between two SAR images was not confirmed apparently. Figs. 12 and 13 show coherence intensity map of respective HH, VH polarized signals. Fig. 14 shows the relationship between P_D and P_N , when using each detection

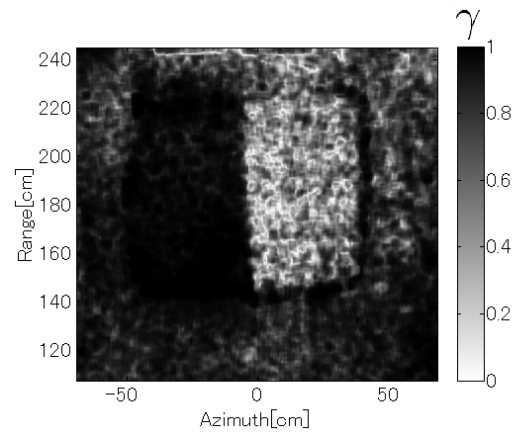


Figure 12. Coherence intensity map of the complex SAR images using the HH polarized signals.

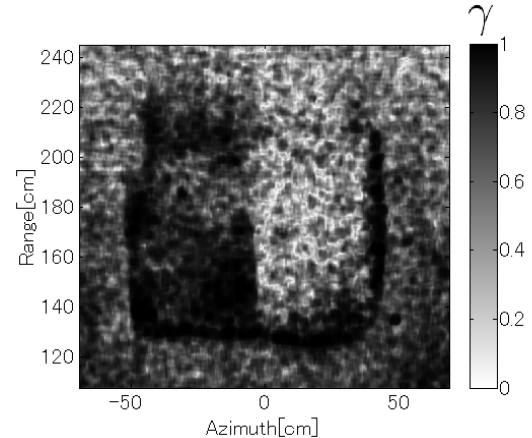


Figure 13. Coherence intensity map of the complex SAR images using the HV polarized signals.

index as the case of HH and HV polarized radiations. The total number of the imaging pixels is 30000. $L = 3$ cm is applied in Eq. (1). Under the limit of the computational burden, the minimum value of P_N is set as 10^{-4} . This figure verifies that the proposed method enhances the detection probability to 8 % in HH, 17 % in VH at the same $P_N = 10^{-3}$. This is only because the proposed detection index β detects the phase difference of γ , which is not considered in the conventional index. Furthermore, the left and right hand side of Fig. 15 shows the distribution of γ on the Gaussian plane and the threshold boundaries determined by the conventional and proposed indices for the HH and HV cases, respectively. As shown in this figure, the proposed boundary is more suitable for the change detection by considering the phase. Next, the performance under the lower SNR situation is investigated. The white Gaussian noises were directly added to the image s_1 and s_2 . Fig. 16 shows the relationship between P_N and P_D in SNR=20dB. From the figure, it is clear that a high detection performance is achieved by considering the phase even under the lower SNR. Fig. 17 shows distribution on the Gaussian plane and the threshold boundaries determined by the conventional and proposed indices for the HH and HV cases,

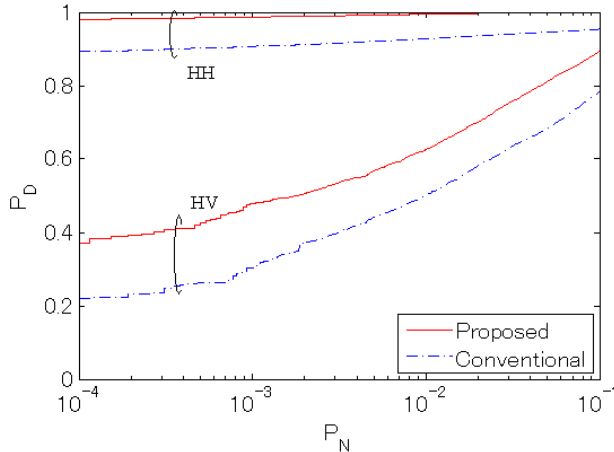


Figure 14. P_N - P_D characteristic with the experimental data.

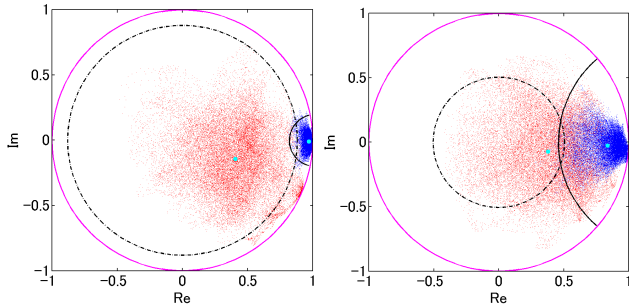


Figure 15. Distribution of γ in the experimental data the experiment using HH (left) and HV (right) polarized signals, respectively.

respectively under the lower SNR. It shows that the unchanged points in Fig. 17 have lower absolute value of γ than that of Fig. 15.

VI. CONCLUSION

This paper proposed a novel detection index for CCD of the complex SAR images. The proposed index detects phase difference of γ , which is not considered in the conventional Fisher's index. The experimental investigation proved that the proposed method provided almost 10 % higher detection probability compared to the conventional method. In the lower SNR situation, where the noises were added numerically, it is confirmed that this method holds a significant advantage for the change detection ability. The future work will focus on how to enhance the spatial resolution of the change detection area by using the spatial domain interferometer, or estimate the height from the obtained phase discrepancy.

ACKNOWLEDGMENT

This work is supported by Information Technology R&D Center, Mitsubishi Electric Corporation.

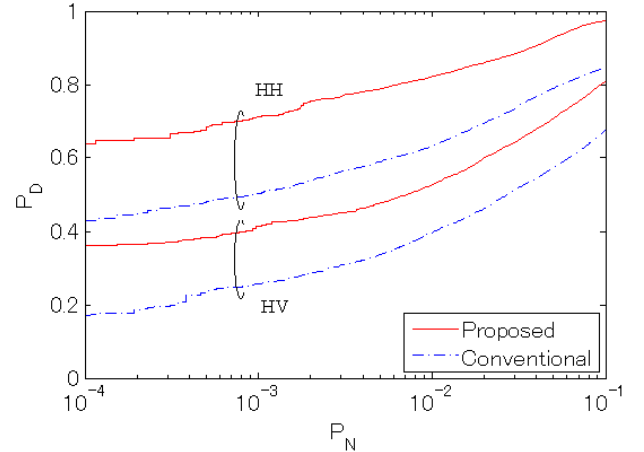


Figure 16. P_N - P_D characteristic with the experimental data, (SNR=20dB).

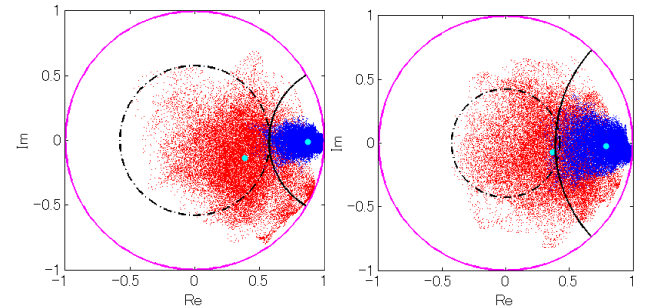


Figure 17. Distribution of γ in the experimental data the experiment using HH (left) and HV (right) polarized signals, respectively.

REFERENCES

- [1] W. M. Brown, "Synthetic aperture radar," *IEEE Trans. Aerosp. Electron. Syst.*, vol. AES-3, pp. 217-229, Mar. 1967.
- [2] L. M. H. Ulander, H. Hellsten and G. Stenstrom, "Synthetic-Aperture Radar Processing Using Fast Factorized Back-Projection," *IEEE Trans. on Aerosp. Electron. Syst.*, vol. 39, no. 3, pp. 760-776, July. 2003.
- [3] R. Goodman, S. Tummala and W. Carrara, "Issues in Ultra-Wideband, Widebeam SAR Image Formation," *In Proceedings of the IEEE International Radar Conference, Washington, D.C.*, pp. 479-485, May. 1995.
- [4] R. Touzi, A. Lopes, J. Bruniquel and P. W. Vachon, "Coherence Estimation for SAR Imagery," *IEEE Trans. Geosci. Remote Sensing*, vol. 37, no. 1, pp. 135-149, Jan. 1999.
- [5] G. Franceschetti and R. Lanari, "Synthetic Aperture RADAR PROCESSING," *New York: CRC Press*, pp. 185-195, 1999.
- [6] H. A. Zebker and J. Villasenor, "Decorrelation in interferometric radar echoes," *IEEE Trans. Geosci. Remote Sensing*, vol. 30, no. 5, pp. 950-959, Sep. 1992.
- [7] E.W. Hoen, H. A. Zebker, "Penetration depths inferred from interferometric volume decorrelation observed over the Greenland Ice Sheet," *IEEE Trans. Geosci. Remote Sensing*, vol. 38, no. 6, pp. 2571-2583, Nov. 2000.
- [8] P. Wright, T. Macklin, C. Willis and T. Rye, "Coherent Change Detection with SAR," *2005 European Radar Conference*, pp. 17-20, Oct. 2005.
- [9] L. Tsang, J. A. Kong, K.-H. Ding and C. O. Ao, "Scattering of Electromagnetic Waves: Numerical Simulations," *New York: Wiley*, pp. 581-590, 2001.